Physica B 454 (2014) 197–203

Contents lists available at ScienceDirect

Physica B

journal homepage: www.elsevier.com/locate/physb

Optical properties and dielectric relaxation of polyvinylidene fluoride thin films doped with gadolinium chloride

Somyia El-Sayed [1]

Physics Department, Faculty of Science, Fayoum University, 63514 El Fayoum, Egypt, and Physics Department, Faculty of Science, Taif University, Saudi Arabia

ARTICLE INFO

Article history:
Received 3 May 2014
Received in revised form
24 July 2014
Accepted 26 July 2014
Available online 7 August 2014

Keywords:
X-ray diffraction
Optical properties
Dielectric relaxations
Conduction mechanism.

ABSTRACT

In this study, the properties of pure and $GdCl_3$-doped polyvinylidene fluoride (PVDF) films were investigated. X-ray diffraction revealed that the PVDF was composed of mixed α and β phases. Adding $GdCl_3$ to PVDF decreased the crystallinity of the polymer matrix. At room temperature, in the ultraviolet-visible range both the absorbance (a) and extinction coefficient (k) of PVDF decreased with $GdCl_3$ content, demonstrating that the optical response of the doped films improved because of increasing optical energy gap (E_g). We also measured the dielectric loss (ε''), electric modulus (M''), and ac conductivity (σ_{ac}) at 300–450 K and 0.1–3000 kHz. The pure and doped PVDF exhibited different relaxation processes. The activation energy (E_a) of the α_c relaxation decreased with increasing $GdCl_3$ content, following an Arrhenius relationship. The behavior of the ac conductivity revealed that the conduction mechanism for studied films followed correlated barrier hopping model. The hopping distance (R) was calculated at different temperatures for all investigated samples.

1. Introduction

Polyvinylidene fluoride (PVDF) has been widely investigated because of its chemical resistance, high dielectric permittivity, and interesting pyroelectric and piezoelectric properties [1–3]. PVDF has been used widely in biotechnology [4], photo-recording [5], microwave modulation, [6] and rechargeable lithium batteries [7]. PVDF exists in two phases: α and β. Polymerization of PVDF from a melt or solution creates the non-polar α-phase with a trans-gauche left-trans gauche right (TGT$\overline{G}$). Kulek et al. reported that the neighboring units of the conformation macromolecules exhibit antiparallel dipole moments [8]. β-PVDF spontaneously polarizes because of parallel alignment of dipoles in neighboring units of the macromolecule, leading to zigzag trans (TTTT) conformation. Because of this conformation, β-PVDF exhibits ferroelectric properties [9].

Rare earth ions can form complexes with polymeric materials because of the ions relatively large size, tendency to form few covalent bonds, and weak electrostatic interactions with negatively charged ligands [10,11]. Because the importance of polymeric composites and complexes has steadily increased, many polymer–metal composites have been studied to understand their physical properties [12,13]. The properties of polymers can be modified by adding fillers to the matrix, which causes interactions between the matrix and filler or the formation of a matrix/filler interface [14,15]. Adding filters to complexes and composites can improve and stabilize their mechanical, electrical, and thermal properties [16,17].

Rare-earth complexes are useful for light-emitting diodes, optical fibers, lasers, optical-signal amplifiers, and other applications. Rare-earth salts also greatly affect the structural, optical, and electrical properties of polymers [18–21]. For example, doping PVDF with metal halides improves the polymer's spectroscopic and physical properties and enhances its optical response [22,23]. However, to our knowledge, little research exists on how rare-earth halides affect the optical properties of PVDF. Because of this knowledge gap, in the present report we studied how $GdCl_3$ affected the optical properties of PVDF films.

We have reported on the effect of rare earth chlorides on the dielectric properties of PVDF thin films [24,25]. It became clear that the type of rare earth ions plays a curial role on the dielectric properties of PVDF. For instance, it was found that the conduction mechanism of PVDF depends on the content of $LaCl_3$ doping [24]. It was found that the addition of $LaCl_3$ to PVDF causes a reduction of the crystallinity due to the crosslinking between La^{3+} and flourine group ($-CF_2$) of PVDF. The temperature and frequency dependence of ε'' of pure PVDF revealed three relaxation processes; ρ-, α_a- and α_c- relaxations. These relaxations were affected by adding $LaCl_3$ to the PVDF matrix. The frequency dependence of the ac conductivity (σ_{ac}) revealed that the correlated barrier hopping (CBH) is the most probable conduction mechanism at α_a-relaxation for both pure PVDF and PVDF doped with 5 and 10 wt.% $LaCl_3$. While the conduction

E-mail address: somyia.elsayed@yahoo.com
[1] Tel.: +966507276346; fax: +966128321071.

http://dx.doi.org/10.1016/j.physb.2014.07.076
0921-4526/

mechanism of 3 wt.% $LaCl_3$-doped PVDF is small polaron tunneling (SPT) type. In addition, there is an order of magnitude difference between the ac conductivity of 3 wt.% $ErCl_3$ and that of the same content of $GdCl_3$-doped PVDF thin films [25]. These results motivated us to investigate the effect of different amount of $GdCl_3$ on the optical properties and dielectric relaxations of PVDF. The reason to study various ratios of $GdCl_3$/PVDF is to compare between the effect of $GdCl_3$ and $LaCl_3$ on the physical properties of PVDF thin films. Because La^{3+} ions are nonmagnetic on contrast to Gd^{3+} ones which exhibit large paramagnetic moment, and also the first is larger in size than the second, it is expected to get a different result in this work.

2. Experimental techniques

PVDF (M_w=53 000) was obtained from Sigma-Aldrich, Steinheim, Germany (code number 81432). Gadolinium chloride ($GdCl_3$; 99.99% purity, trace metals basis; product number 439770) was also obtained from Sigma-Aldrich. PVDF films with varying amounts of $GdCl_3$ (wt.%) were prepared by casting as follows. First, PVDF was dissolved in *N-N* dimethylformamide (reagent grade, Aldrich) at 90 °C for 30 min. $GdCl_3$ was then dissolved in pure ethanol and added to the polymeric solution. The solutions remained at 90 °C until they reached a suitable viscosity. When the solids completely dissolved, the solutions were allowed to cool to 50–60 °C for 8 h while being stirred continuously. The mixtures were cast onto glass dishes and kept in a furnace at 50 °C for 24 h and then at room temperature (34 °C) for 6 days to ensure complete evaporation of the solvent. The thickness of the obtained films was ≈0.11 mm. PVDF films filled with weight fractions (W) of 0%, 5%, 7%, and 10% were fabricated. The weight fraction was calculated as follows:

$$W(wt.\%) = \frac{w_f}{(w_p + w_f)} x\ 100 \quad (1)$$

where w_f and w_p are the weights of the $GdCl_3$ and PVDF, respectively. A trail has been done to prepare films with concentration higher than 10 wt.% $GdCl_3$ but the homogeneity of the films were not good and so that they were excluded from this work.

Optical characterization was performed using a spectrophotometer (Shimadzu UV-3600 UV–vis-NIR) at 200–850 nm with an accuracy of ±0.2 nm. X-ray diffraction (XRD) was performed at room temperature using CuK_α radiation (Rigaku Miniflex). Dielectric measurements were performed using an LCR tester (Hioki model 3532 High Tester LCR; Ueda, Nagano, Japan) with a capacitance accuracy of ±0.0001 pF. Temperature was measured with a T-type thermocouple, with its junctions barely contacting the sample, and accuracy better than ±1 °C. The complete frequency range was scanned during heating by using a computer program. The samples were coated with silver paste to produce ohmic contacts. The dielectric permittivity (ε') of each sample was calculated as $\varepsilon' = dC/\varepsilon_o A$, where C is the capacitance, d is the sample thickness, ε_o is the permittivity of free space, and A is the cross-sectional area of the sample. The total ac conductivity (σ_t) was obtained using $\sigma_t = 2\pi f \varepsilon_o \varepsilon''$, where ε'' is the dielectric loss. The ac conductivity (σ_{ac}) was corrected from the low-frequency conductivity (σ_{dc}) as given in Eq. (9).

3. Results and discussion

3.1. X-ray diffraction

Fig. 1 shows XRD patterns of pure PVDF and PVDF doped with 10 wt.% $GdCl_3$, which exhibited a semicrystalline structure. Pure PVDF exhibited a peak at $2\theta \approx 20.4°$, corresponding to diffraction

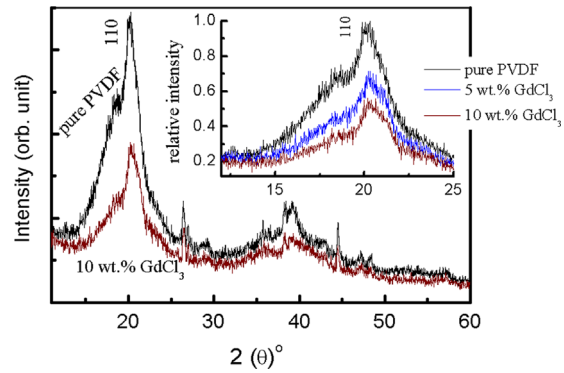

Fig. 1. XRD patterns of pure and 10 wt.% $GdCl_3$-doped PVDF. The inset shows the X-ray maximum diffraction peak of pure and $GdCl_3$-doped PVDF.

from (110) of β-PVDF [22,26]. It also exhibited peaks at $2\theta \approx 26.56°$, 35.75°, 38.62°, and 40°, suggesting the presence of α–PVDF [27]. Overall, pure PVDF exhibited mixed α- and β-PVDF crystalline phases [22,28]. Doping PVDF with $GdCl_3$ decreased the XRD peak intensities with increasing doping, as shown in the inset of Fig. 1, suggesting that adding $GdCl_3$ decreased the ordering of the crystalline PVDF because of crosslinking in the crystalline and amorphous regions; other reports have shown that polymer crosslinking often reduces crystallinity [29–31]. Adding $GdCl_3$ also shifted the main reflection PVDF peak slightly with increasing Gd content, as shown in the inset of Fig. 1. The decrease in the maximum intensity with $GdCl_3$ content gives information on decreasing the crystallinity of the PVDF. Probably, doping PVDF by $GdCl_3$ reflects a strain-dependent crystallinity within the polymer matrix. This strain-dependent crystallinity can be attributed to the crosslinking between Gd^{3+} and flourine group ($-CF_2$) of PVDF.

3.2. Optical properties

Fig. 2(a) shows the ultraviolet-visible (UV–vis) absorption (α) spectra of pure and $GdCl_3$-doped PVDF, showing that adding $GdCl_3$ decreased α. We observed an absorption band at ≈277 nm for both pure and doped PVDF [32]. For the pure PVDF, we observed no other absorption peaks at higher wavelengths, in agreement with Abdelrazek et al. [22]. For all the $GdCl_3$-doped PVDF films, though, we observed another band at ≈317 nm. For the doped PVDF films with 5 and 10 wt.% $GdCl_3$, we also observed additional peaks at 379 and 520 nm. The shift in the absorption edge of the doped PVDF reflects the variation in the energy band gap, which may have been caused by varying crystallinity in the polymer matrix or by the formation of charge transfer complexes, as reported for $AgNO_3$-doped polyvinyl alcohol (PVA) [33]. To more clearly view these absorption bands, we calculated the extinction coefficient (k) [34] as follows:

$$k = \frac{\lambda a}{4\pi} \quad (2)$$

where a is the absorption coefficient, which is defined as the absorbance (A) per unit film thickness (d); Fig. 2(b) shows k plotted versus wavelength (λ). We calculated a as follows:

$$a = \frac{A}{d} \quad (3)$$

Note that k decreased with $GdCl_3$ content. Using the UV–vis spectra, we determined the optical energy band gap (E_g) according to the frequency dependence of the absorption coefficient, a

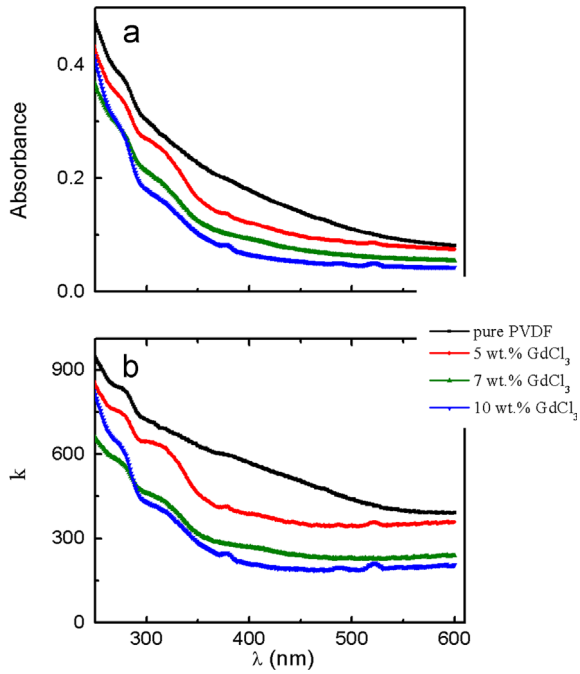

Fig. 2. (a,b): (a) UV–vis spectra of pure and $GdCl_3$-doped PVDF. (b) The extinction coefficient (k) of pure PVDF and $GdCl_3$-doped PVDF films.

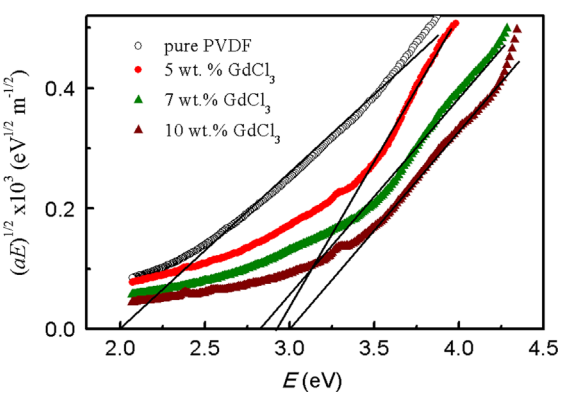

Fig. 3. Optical energy band gap (E_g) of pure PVDF and $GdCl_3$-doped PVDF samples.

[35,36]:

$$a(\nu) = \frac{\beta_0 (h\nu - E_g)^c}{h\nu} \tag{4}$$

where c is an empirical index equal to 1/2 for a quantum mechanically allowed direct transition during optical absorption and β_0 is a constant. The plot of $(ah\nu)^{1/2}$ versus $h\nu$ at room temperature, as shown in Fig. 3, allowed us to estimate E_g by extrapolating the linear part of $(ah\nu)^{1/2}$ to zero in the range of 2 eV $< E <$ 4.3 eV. Increasing $GdCl_3$ doping also increased E_g, as shown in Table 1. This behavior is ascribed to the negative effect of $GdCl_3$ on the crystallinity of PVDF. Pure PVDF exhibited an E_g of $\approx$2 eV, a higher value than previously reported [22]. The variation of E_g with added $GdCl_3$ may have been caused by interactions between Gd^{3+} ions and CF_2 groups of PVDF.

4. Dielectric relaxation

4.1. Dielectric loss factor

Fig. 4(a–d) shows how the dielectric loss factor (ε'') depended on frequency for pure and doped PVDF at various temperatures. ε'' decreased monotonically with increasing frequency but increased with increasing $GdCl_3$ content, except at 5 wt.%. This behavior emphasizes that incorporating $GdCl_3$ increased the amount of amorphous PVDF, in agreement with XRD. Within the studied temperature and frequency ranges, we only found a $\varepsilon''(f)$ peak in 5 wt.% $GdCl_3$-doped PVDF at low frequencies. This peak was caused by the glass transition temperature (T_g) of PVDF which occurs at low frequencies and $T <$ 320 K. At frequency ($f \approx$ 3.2 kHz), another peak is observed for pure PVDF, and PVDF doped with 5 and 7 wt.% $GdCl_3$. This peak can be attributed to α_a-relaxation and it is not observed in 10 wt.% $GdCl_3$-doped PVDF film. In addition, we found no ρ peak in the $\varepsilon''(f)$ plots of the doped samples. Note that the dielectric loss of 5 wt.% $GdCl_3$-doped PVDF was lower than in the other samples. Probably, this concentration of $GdCl_3$ is effective, and similar to that reported on 0.5 wt.% ZnO-doped polyvinyl alcohol (PVA) [37]. Moreover, we ascribe the differences in behavior of the pure PVDF in the present and our previous reports [24,25] to the differences in molecular atomic weight and the studied PVDF in this work composed of two phases (α and β).

Table 1
Optical energy gap (E_g), relaxation time at infinite temperature (τ_o), and activation energy (E_a). of α_c-relaxation (obtained by fitting to Eq.(8)) for pure and $GdCl_3$-doped PVDF.

Sample	E_g (eV)	$\ln(\tau_o/s)$	E_a (eV)
pure PVDF	2.0	-34 ± 0.93	0.81 ± 0.03
5 wt.% $GdCl_3$	2.94	-27 ± 2.53	0.61 ± 0.08
7 wt.% $GdCl_3$	2.85	-23 ± 0.81	0.41 ± 0.06
10 wt.% $GdCl_3$	3.02	-22 ± 0.37	0.37 ± 0.01

Fig. 5(a–d) shows how ε'' depends on temperature for pure and doped PVDF at various frequencies. For pure PVDF, ε'' increased gradually with temperature and decreased with increasing frequency. We observed similar behavior in all $GdCl_3$-doped PVDF samples as well as a peak at $\approx$400 K. This peak was also caused by α_c-relaxation, due to dipolar motion of the polymer backbones in the crystalline regions. As the frequency increased, the peak height increased and the peak position shifted to higher temperatures. For the 5 wt.% $GdCl_3$-doped PVDF, we observed another peak at $\approx$360 K, which was caused by α_a-relaxation. This behavior may have been caused by micro-Brownian dipolar motion of the polymer backbones in the amorphous region.

4.2. Electric modulus

Interfacial polarization is almost always present in polymer composites, but it is hidden by the conductivity of the composite. Nevertheless, this polarization causes the dielectric permittivity to be high at low frequencies and high temperatures. To overcome the difficulty of observing the interfacial polarization, the modulus formulism can be used to analyze the electrical conductivity in an ionic polymeric material. The modulus formalism can also be used to suppress the signal intensity associated with electrode polarization, emphasizing small features at high frequencies. Because of these advantages, this technique has been commonly used to determine charge carrier parameters, including the conductivity relaxation time [38–40]. The dielectric measurements can be expressed in terms of the complex electric modulus (M^*), which is defined as the inverse of the complex permittivity (ε^*):

$$M^* = \frac{1}{\varepsilon^*} = \frac{\varepsilon'}{\varepsilon'^2 + \varepsilon''^2} + i\frac{\varepsilon''}{\varepsilon'^2 + \varepsilon''^2} \tag{5}$$

or

$$M^* = M' + iM'' \tag{6}$$

where M' and M'' are the real and imaginary parts of the electric modulus, respectively.

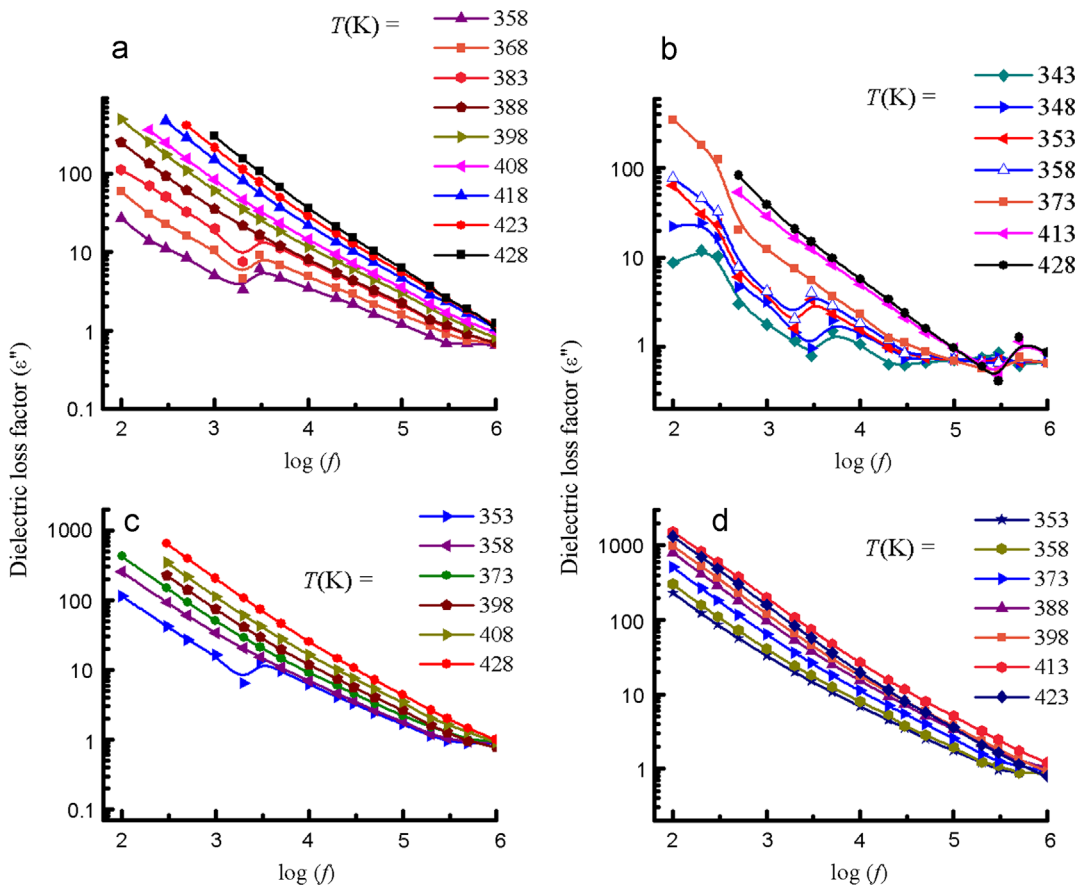

Fig. 4. (a–d): Frequency dependence of ε'' at various temperatures for: (a) pure PVDF, (b) 5 wt.% $GdCl_3$-doped PVDF, (c) 7 wt.% $GdCl_3$-doped PVDF, and (d) 10 wt.% $GdCl_3$-doped PVDF.

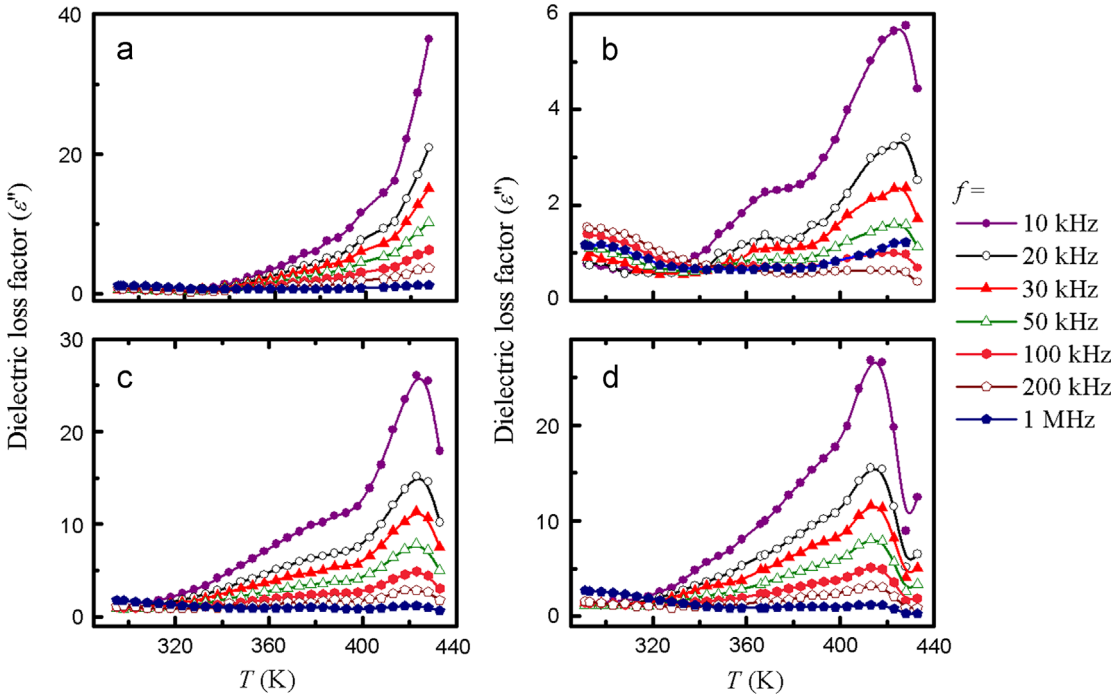

Fig. 5. (a–d): Temperature dependence of ε'' at various frequencies for: (a) pure PVDF, (b) 5 wt.% $GdCl_3$-doped PVDF, (c) 7 wt.% $GdCl_3$-doped PVDF, and (d) 10 wt.% $GdCl_3$-doped PVDF.

Fig. 6(a–d) shows how M'' depended on frequency for pure and doped PVDF at various temperatures. Both pure and doped PVDF exhibited α_c relaxation at higher temperatures, a peak which shifted to higher frequencies with increasing temperature. As discussed before, this behavior is caused by molecular motion of polymer backbone in the crystalline region below the melting temperature.

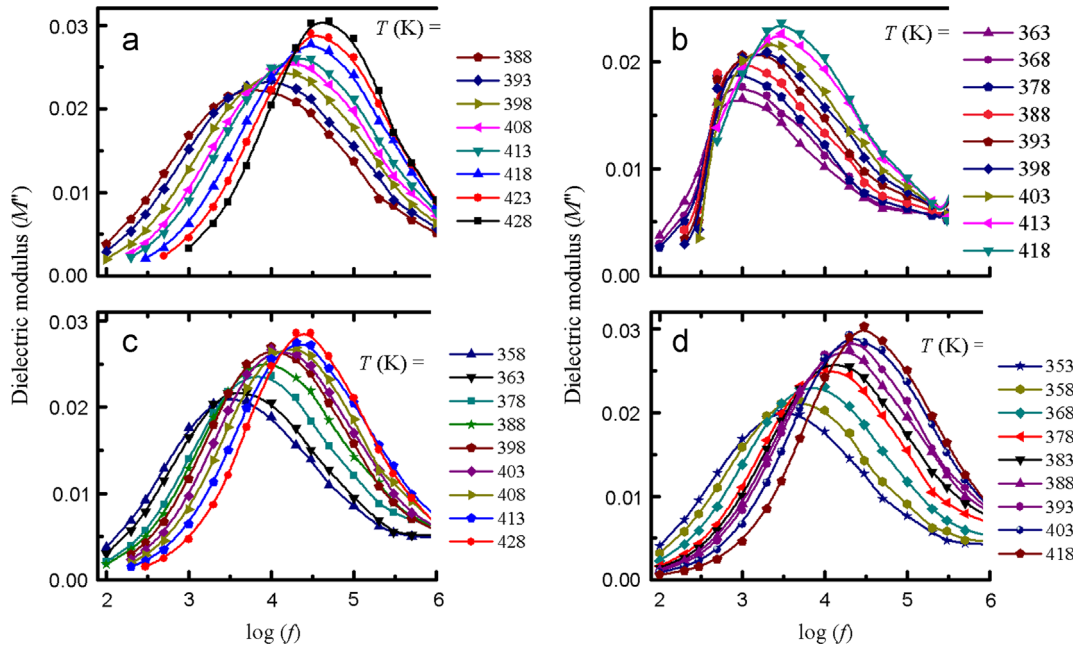

Fig. 6. (a–d): Frequency dependence of the imaginary part of the electric modulus, M'', at various temperatures for: (a) pure PVDF, (b) 5 wt.% $GdCl_3$-doped PVDF, (c) 7 wt.% $GdCl_3$-doped PVDF, and (d) 10 wt.% $GdCl_3$-oped PVDF.

Using the electric modulus formalism addition, we also observed enhancement of the contribution of dc conductivity effects (at low frequencies). Owing to the contribution of interfacial polarization, this α_c relaxation occurs at the interfaces between Gd^{3+} ions and the polymer matrix. The low-frequency side of this M'' peak signifies the range in which ions can successfully hop to neighboring sites, while the high-frequency side represents the range in which the ions are spatially confined to their potential wells and can only move within the well. Thus, the region of the peak occurs indicates the transition from long-range to short-range mobility with increasing frequency. The bell shape of this peak is also typical of ionic materials [41]. The shape of M'' might also indicate that the conduction mechanism is temperature-dependent hopping [42]. In contrast, the α_c-relaxation peak does not appear clearly for $LaCl_3$-doped PVDF [24]. This deviation is further evidence that the chemical nature and electronic configuration of the rare-earth ion dopants play important roles in the physical properties of these polymer complexes. The full width at half maximum of this α_c peak decreased with increasing temperatures because of deviations in the high-frequency side of the peak. The electric-field relaxation caused by charge carrier motion is generally well described by the empirical Kohlrausch–Williams–Watts function [40,43]:

$$\phi(t) = \exp(-t/\tau)^{\gamma},\ 0 < \gamma \leq 1 \tag{7}$$

where β is Kohlrausch exponent. As γ decreases, the relaxation behavior deviates from Debye-type relaxation (occurring at $\gamma = 1$). A similar behavior has been reported for PVDF composites [44].

The frequency where M'' is maximum (f_m) defines the relaxation time (τ) by $2\pi f_m \tau = 1$. Psarras et al. found that τ exhibited Arrhenius behavior [45]:

$$\tau = \tau_o \exp\left(\frac{E_a}{kT}\right) \tag{8}$$

where E_a is the activation energy of the relaxation process, τ_o is the relaxation time at infinite temperature, k is the Boltzmann constant, and T is the absolute temperature. Fig. 7 plots $\ln(\tau)$ vs. 1000/T for pure and doped PVDF films, and Table 1 shows the calculated values of E_a and τ_o for pure and doped PVDF. These E_a values indicate that the conduction mechanism is ionic, similar to the mechanism reported for PVA doped with rare-earth ions [46]. Furthermore, the fitting parameter (τ_o) we obtained for pure PVDF agrees with previous reports [47,48]. In addition, the values of τ_o increased with $GdCl_3$ content.

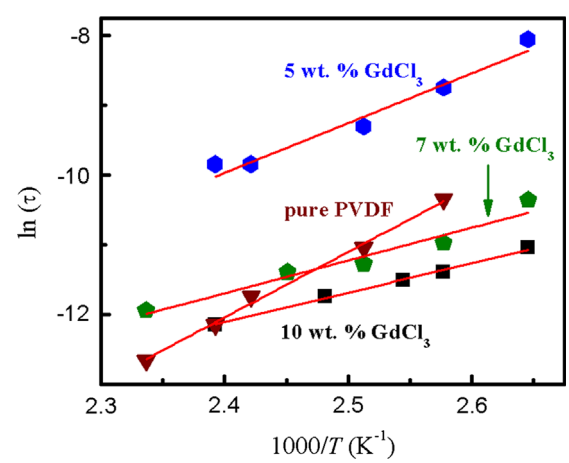

Fig. 7. $\ln(\tau)$ vs. 1000/T for pure and $GdCl_3$-doped PVDF. The solid red lines show the fits to Eq. (8).

Fig. 8(a–d) shows how M'' depended on temperature for pure and doped PVDF at various fixed frequencies. The M'' of pure PVDF exhibited two peaks, as shown in Fig. 8(a). As discussed before, the first peak was caused by α_a relaxation, which occurs near room temperature. This peak appears as a hump in $GdCl_3$-doped PVDF at higher frequencies. We observed a second peak in all samples at ≈ 400 K, caused by α_c relaxation, which shifted towards higher temperatures with increasing frequency.

4.3. AC conductivity

The frequency dependence of the ac conductivity (σ_{ac}) can be described as [49,50]:

$$\sigma_{ac}(f) = \sigma_t - \sigma_{dc} = 2\pi B f^s \tag{9}$$

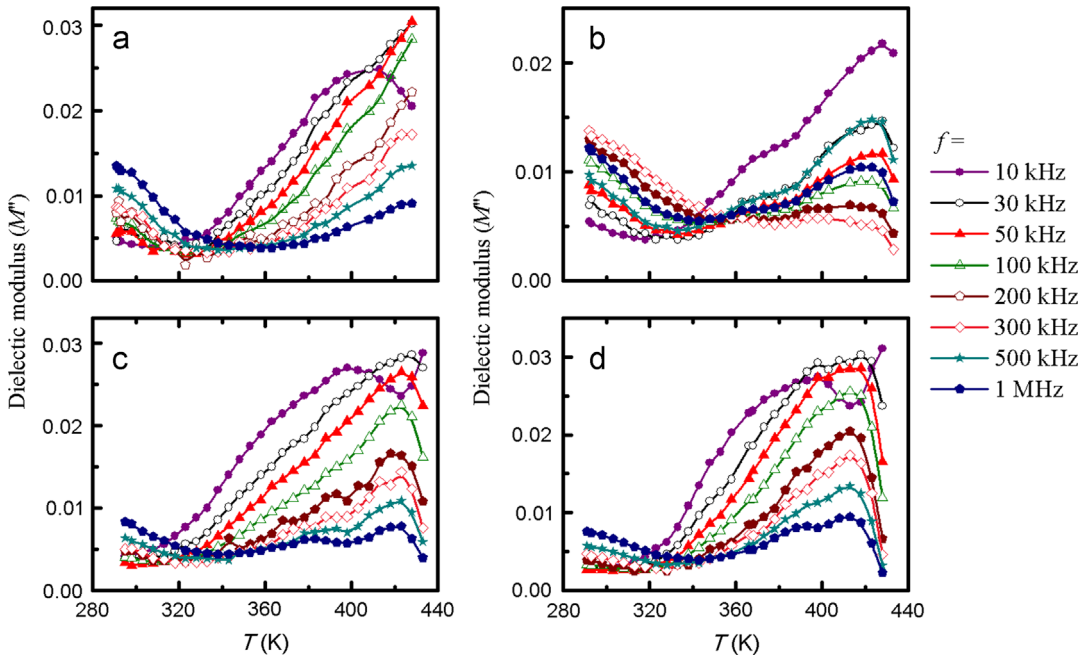

Fig. 8. (a–d): Temperature dependence of the imaginary part of the electric modulus (M'') at various frequencies for: (a) pure PVDF, (b) 5 wt.% $GdCl_3$-doped PVDF, (c) 7 wt.% $GdCl_3$-doped PVDF, and (d) 10 wt.% $GdCl_3$-doped PVDF.

where σ_{dc} is the low-frequency conductivity, σ_t is the total conductivity, s is a universal exponent, and B is a pre-exponential factor. The dc conductivity is subtracted by extrapolating $\sigma_t(f)$ to $f \rightarrow 0$. To identify the dominant conduction mechanism, we considered the frequency dependence of σ_{ac} within the frequency range of α_c relaxation, as shown in Fig. 9(a–c). These results yield straight lines with different slopes (i.e., different s). Table 2 shows s and log (B) for pure and doped PVDF films at various temperatures. Because s decreased with increasing temperature, we believe the conduction mechanism to be correlated barrier hopping [51]. Compared with $LaCl_3$-doped PVDF with the same doping range (except for 3 wt.%), s has been shown to decrease with increasing temperature [24]. This similarity suggests that, over a similar doping range, the conduction mechanism of $LaCl_3$-doped PVDF is similar to that of $GdCl_3$-doped PVDF. The hopping distance (R) was calculated based on the universal exponent, s, as [41,52]:

$$R = \frac{6kT}{1-s} \tag{10}$$

where k is the Boltzmann constant, and T is the absolute temperature. The values of R for pure PVDF and $GdCl_3$-doped films were calculated at different temperatures and listed in Table 2. It is noticed that the values of R decreased with increasing $GdCl_3$ content.

5. Conclusions

Our XRD results show that both pure and doped PVDF were composed of mixed, crystalline α- and β-PVDF. Adding $GdCl_3$ reduced the crystallinity of the polymer because of increased crosslinking density. Doping the films increased their optical energy gap (E_g). Increasing the $GdCl_3$ content also decreased both a and k. Our measurements of the temperature and frequency dependence of ε'' of pure PVDF revealed two relaxation processes in the temperature and frequency ranges we studied. The first is α_a relaxation, which we attribute to micro-Brownian motion of the polymer backbones in the amorphous region. The second is α_c relaxation, occurring at higher temperatures, which we attribute to molecular motion of the polymer backbones in the crystalline region. The temperature dependence of the relaxation time for α_c relaxation followed an Arrhenius relationship. We attribute the enhancement of M'' by adding $GdCl_3$ to interfacial polarization and

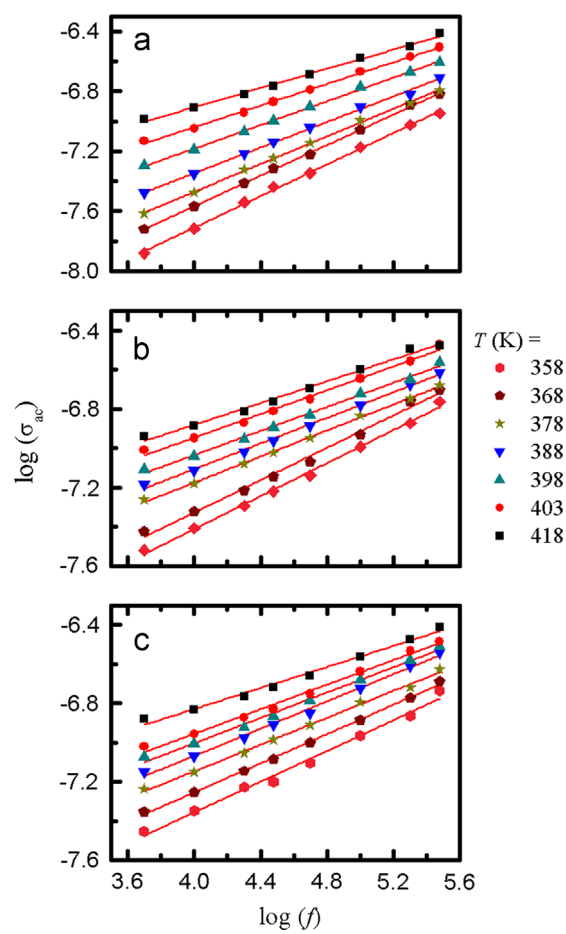

Fig. 9. (a–c): Frequency dependence of σ_{ac} for: (a) pure PVDF, (b) 7 wt.% $GdCl_3$-doped PVDF, and (c) 10 wt.% $GdCl_3$-doped PVDF. The solid red lines show the fits to Eq. (9).

Table 2
Frequency exponent (s), pre-exponential factor (B), fit to Eq. (9), and the hopping distance (R) according to Eq. (10) for pure and $GdCl_3$-doped PVDF at various temperatures.

T (K)	Pure PVDF			5 wt.% $GdCl_3$			7 wt.% $GdCl_3$			10 wt.% $GdCl_3$		
	log B	s	R (eV)	log B	s	R (eV)	log B	s	R (eV)	log B	s	R (eV)
358	-9.82 ± 0.04	0.53	**0.394**	-9.89 ± 0.23	0.47	**0.349**	-9.09 ± 0.05	0.42	**0.319**	-8.92 ± 0.07	0.39	**0.303**
368	-9.61 ± 0.03	0.51	**0.388**	-9.47 ± 0.18	0.44	**0.339**	-8.98 ± 0.07	0.41	**0.322**	-8.74 ± 0.03	0.37	**0.302**
378	-9.41 ± 0.03	0.46	**0.362**	-9.35 ± 0.21	0.39	**0.320**	-8.70 ± 0.06	0.38	**0.315**	-8.51 ± 0.04	0.34	**0.296**
388	-9.06 ± 0.04	0.43	**0.352**	-9.34 ± 0.19	0.37	**0.318**	-8.50 ± 0.02	0.37	**0.318**	-8.45 ± 0.05	0.34	**0.303**
398	-8.76 ± 0.02	0.39	**0.337**	-9.25 ± 0.16	0.35	**0.316**	-8.41 ± 0.03	0.33	**0.307**	-8.29 ± 0.04	0.32	**0.302**
403	-8.56 ± 0.03	0.37	**0.330**	-9.10 ± 0.17	0.33	**0.310**	-8.16 ± 0.05	0.32	**0.306**	-8.20 ± 0.05	0.31	**0.301**
418	-8.19 ± 0.04	0.36	**0.337**	-8.98 ± 0.12	0.32	**0.317**	-7.99 ± 0.05	0.28	**0.300**	-7.90 ± 0.06	0.27	**0.296**

increased dc conductivity. Finally, by investigating σ_{ac}, we revealed that the most probable conduction mechanism for both the pure and doped PVDF films was correlated barrier hopping. The hopping distance, R, decreased with increasing the content of $GdCl_3$ because of the crosslinking between Gd^{3+} ions and CF_2 of PVDF.

Acknowledgments

The author would like to thank the staff of the Physics Department, Faculty of Science, Fayoum University, for their help and fruitful discussions.

References

[1] W.A. Yee, M. Kotaki, Y. Liu, X. Lu, Polym 48 (2007) 512–521.
[2] M. Wang, J.H. Shi, K.P. Pramoda, S.H. Goh, Nanotechnology 18 (23) (2007) 235701.
[3] F. He, F. Fan, S. Lau, Polym. Test. 27 (8) (2008) 964.
[4] L.-P. Cheng, D.-J. Lin, C.-H. Shih, A.-H. Dwan, C.C. Gryte, J. Polym. Sci. Part B: Poly. Phys 37 (1999) 2079.
[5] A. Tawansi, A.H. Oraby, E. Ahmed, E.M. Abdelrazek, M. Abdelaziz, J. Appl. Polym. Sci 70 (1998) 1759–1767.
[6] A. Tawansi, M.I. Ayad, E.M. Abdelrazek, J. Appl. Polym. Sci 72 (1999) 771–781.
[7] K.M. Kim, N.-G. Park, K.S. Ryu, S.H. Chang, Polym 43 (2002) 3951–3957.
[8] J. Kulek, I. Szafraniak, B. Hilczer, M. Polomska, J. Non-Cryst. Solids 353 (2007) 4448–4452.
[9] T. Furukawa, G.E. Johnson, Appl. Phys. Lett. 38 (1981) 1027.
[10] M. Takahashi, Y. Hara, K. Aoshima, H. Kurihara, T. Oshikawa, M. Yamashita, Tetrahedron Lett. 41 (44) (2000) 8485–8488.
[11] M.C. Silva, A.S.S. de Camargo, L.A.O. Nunes, R.A. Silva, A. Marletta, J. Non-Cryst. Solids 354 (2008) 5496–5503.
[12] L.O. Faria, R.L. Moreira, J. Polym. Sci. Part B: Polym. Phys 37 (1999) 2996–3002.
[13] T. Nagasawa, Y. Murata, K. Tadano, R. Kawai, K. Ikehara, S. Yano, J. Material Sci 35 (12) (2000) 3077–3082.
[14] T. Tanaka, IEEE Trans. Dielect. Electr. Insul 12 (2005) 914.
[15] T.J. Lewis, IEEE Trans. Dielect. Electr. Insul 1 (1994) 812.
[16] D.K. Das-Gupta, K. Doughty, Thin Solid Films 158 (1988) 93–105.
[17] H.L.W. Chan, Q.Q. Zhang, W.Y. Ng, C.L. Choy, IEEE Trans. Dielect. Electr. Insul 7 (2000) 204–207.
[18] F. Xie, Z. Zheng, Physica B 349 (2004) 415–419.
[19] H. Suzuki, Y. Hattori, T. Lizuka, K. Yuzawa, N. Matsumoto, Thin Solid Films 438 (2003) 288–293.
[20] H. Huang, B. Yan, Mater. Sci. Eng. B 117 (2005) 261.
[21] G.A. Kumar, Mater. Lett. 55 (2002) 364–369.
[22] E.M. Abdelrazek, R. Holze, Physica B 406 (2011) 766–770.
[23] M. Abdelaziz, J. Magnet. Magnet. Mater 279 (2004) 184–194.
[24] A. Hassen, T. Hanafy, S. El-Sayed, A. Himanshu, J. Appl. Phys 110 (2011) 114119.
[25] S. El-Sayed, T.A. Abdel-Baset, A. Hassen, AIP Adv. 4 (2014) 037114–037115.
[26] B. Mohammadi, A.A. Yousef, S.M. Bellah, Polym. Test 26 (2007) 42.
[27] C. Muralidhar, P.K.C. Pillal, J. Mater. Sci 23 (1988) 410–414.
[28] G.T. Davis, J.E McKinney, M.G. Broadhust, S.C. Roth, J. Appl. Phys 49 (1978) 4998.
[29] S.A. Nouh, A. Mohamed, H.M. El Hussieny, T.M. Hegazy, J. Appl. Poly. Sci 109 (2008) 3447.
[30] M. Schenk, S. Dauer, T. Lessle, B. Ploss, Ferroelectrics 127 (1992) 215–220.
[31] S.A. Nouh, A. Abdel Naby, H.M. El Hussieny, Appl. Radiat. Isoto 65 (2007) 1173–1178.
[32] A. El-Khodary, M. Abdelaziz, G.M. Hassan, Inter. J. Polym. Mater. 54 (2005) 633–650.
[33] C.U. Devi, A.K. Sharma, V.V.R.N. Rao, Mater. Lett. 56 (2002) 167.
[34] T.J. Alwan, M.A. Jabbar, J. Turk, Phys 34 (2010) 107.
[35] N.F. Mott, E.A. Davis, Electronic Process in Non-crystalline Materials, second ed., Oxford University Press, Oxford, (1979) 273.
[36] J. Tauc, Optical Properties of Solid (A. Abeles, Amsterdam, North Holland) 1972, p. 277.
[37] A.S. Roy, S. Gupta, S. Sindhu, A. Parveen, P.C. Ramamurthy, Composites, Part B 47 (2013) 314–319.
[38] R. Richert, J. Non-Cryst. Solids 305 (1–3) (2002) 29–39.
[39] F. Kremer, A. Schönhals, Broadband Dielectric Spectroscopy, Springer, Berlin, 2003.
[40] H. Lu, X. Zhang, H. Zhang, J. Appl. Phys 100 (2006) 054104.
[41] M.F. Mostafa, A. Hassen, Phase Transit. 79 (2006) 305–321.
[42] G.M. Tsangaris, N. Kouloumbi, S. Kyvelidis, Mater. Chem. Phys. 44 (3) (1996) 245–250.
[43] K.L. Ngai, S.W. Martin, Phys. Rev. B 40 (1989) 10550.
[44] A.C. Lopes, C.M. Costa, R. Sabater i Serra, I.C. Neves, J.L. Gomez Ribelles, S Lanceros-Méndez, Solid State Ionics 235 (2013) 42–50.
[45] G.C. Psarras, E. Manolakaki, G.M. Tsangaris, Compos. Part A: Appl. Sci. Manufact 34 (2003) 1187.
[46] T.A. Hanafy, J. Appl. Phys 112 (3) (2012) 034102.
[47] C.V. Chanmal, J.P. Jog, eXPRESS Polym. Lett **2** (4) (2008) 294–301.
[48] E. Tuncer, M. Wegener, R. Gerhard-Multhaupt, J. Non-Cryst. Solids 351 (2005) 2917–2921.
[49] N.F. Mott, E.A. Davis, Electronic Processes in Non-crystalline Materials, Oxford University Press, London, 1979.
[50] A.K. Jonscher, Dielectric Relaxation in Solids, Chelsea Dielectric Press, London, (1983) 340.
[51] G.E. Pike, Phys. Rev B 6 (1972) 1572.
[52] R Singh, J. Kumar, R.K. Singh, A. Kaur, R.D. P. Sinha, N.P. Gupta, Polymer 47 (2006) 5919–5928.